electronics

MDPI

Article

Artificial Neural Network for Photonic Crystal Band Structure Prediction in Different Geometric Parameters and Refractive Indexes

Fu-Li Hsiao [1], Hsin-Feng Lee [1], Su-Chao Wang [1], Yu-Ming Weng [1] and Ying-Pin Tsai [2,*]

[1] Institute of Photonics, National Changhua University of Education, Changhua 50007, Taiwan; fulihsiao@cc.ncue.edu.tw (F.-L.H.); d1126003@mail.ncue.edu.tw (H.-F.L.); d0826003@mail.ncue.edu.tw (S.-C.W.); d0426004@mail.ncue.edu.tw (Y.-M.W.)

[2] Institute of Imaging and Biomedical Photonics, College of Photonics, National Yang Ming Chiao Tung University, Tainan 71150, Taiwan

* Correspondence: yingpintsai@gmail.com or j61011tim.pt06@nycu.edu.tw

Abstract: In this study, an artificial neural network that can predict the band structure of 2-D photonic crystals is developed. Three kinds of photonic crystals in a square lattice, triangular lattice, and honeycomb lattice and two kinds of materials with different refractive indices are investigated. Using the length of the wave vectors in the reduced Brillouin zone, band number, r/a ratio, and the refractive indices as the dataset, the desired ANN is trained to predict the eigenfrequencies of the photonic modes and depict the photonic band structures with a correlation coefficient greater than 0.99. By increasing the number of neurons in the hidden layer, the correlation coefficient can be further increased over 0.999.

Keywords: photonic crystal; artificial neural network; band structure

Citation: Hsiao, F.-L.; Lee, H.-F.; Wang, S.-C.; Weng, Y.-M.; Tsai, Y.-P. Artificial Neural Network for Photonic Crystal Band Structure Prediction in Different Geometric Parameters and Refractive Indexes. *Electronics* **2023**, *12*, 1777. https://doi.org/10.3390/electronics12081777

Academic Editor: Nakkeeran Kaliyaperumal

Received: 21 March 2023
Revised: 6 April 2023
Accepted: 7 April 2023
Published: 9 April 2023

1. Introduction

Photonic crystals (PC), artificial materials with a spatially modulated refractive index distribution [1,2], have been widely studied in the past decade. Usually, PCs are designed to have two refractive indexes, the main material with air holes drilled in and pillars with another material built on the substrate. The refractive index then varies with the material periodically in space. With a designed refractive index distribution, a PC can exhibit unusual dispersion behaviors such as negative refraction and photonic band gaps. To investigate these phenomena, the dispersion relationship of a PC, known as the photonic band structure (BS) [3], is depicted, revealing the eigenmodes and the eigenfrequencies corresponding to the k vector. The photonic BS is inspired by the investigation of electronic energy level in the semiconductor region and will be affected by the contrast and the distribution of the refractive indices that are contributed to by the materials and the geometric configuration.

The well-used methods for calculating the photonic BS are known as the plane wave expansion method (PWEM), finite element method (FEM), and finite difference time domain method (FDTD). Based on Bloch's theorem, a wave function propagating in a periodic structure has the same periodicity as the structure. Taking FEM as an example, the photonic BS can be obtained by solving eigenproblems within a unit cell of the corresponding PC. In the simulation, the Floquet boundary condition is applied at corresponding boundaries in pairs to realize the phase delay calculated by Bloch's theorem. By varying the phase difference of the Floquet boundary condition, we can calculate the BS within a reduced Brillouin zone.

In the research of PCs, the photonic BS is the major feature necessary to first understand the dispersion relation of the designed PC. Based on the arrangement of the holes or pillars, PCs can be formed in a square lattice, triangular lattice, or even a honeycomb lattice. Due to

the different lattice constant vectors in the different lattices, the calculation conditions of the BSs are slightly different, and the exhibited features will also be different. For instance, the photonic band gap is a special phenomenon that provides a frequency range with empty eigenroots in the BS. Of the three kinds of mentioned PC lattices, the honeycomb lattice is the one that has the highest chance of producing a complete bandgap. Electromagnetic waves within the band gap range cannot propagate through the PCs, making the PC structures act similar to mirrors. Therefore, by creating spatial defects in the periodic structures, the light can be trapped by the PC and form a cavity region. On the other hand, some bands in the BS can be found in flat line shapes, representing low group velocities, meaning that the slow light effect can also be observed by depicting the BSs. Therefore, a desired BS is important for designing physics phenomena in PCs. However, the modes in BS, which vary with the geometric and material parameters, are not intuitive and linear. The desired BSs can only be obtained by trying many parametric combinations. In addition, the simulation of a BS is a time-consuming process. The requirements for computers may also be harsh for complex structures.

In recent years, deep learning and artificial neural networks (ANN) have attracted extensive attention in all research categories and have also been applied to many optical and electromagnetic studies [4–6]. Several studies have adopted deep learning for designing optical devices and further solving problems inversely. Designing optical devices usually requires a bundle of iterative calculations, is not intuitive, and is highly dependent on the researcher's experience. Fortunately, ANNs are good at handling nonlinear and complex problems and are also simple to design. A well-trained ANN usually saves much computing time compared to traditional calculation methods. Most important of all, deep learning and ANNs reveal a great possibility to inversely design an optical device, i.e., the ANN can be used to design PC devices based on specifications determined by users.

In this study, we aimed to train ANNs to predict the BSs of 2-D PCs. The Levenberg–Marquardt backpropagation method was used in the ANN. The Bayesian regression method was also considered for complex problems. However, the Bayesian regression method did not divide the validation group from the input dataset and cost more training time to obtain a similar result as the Levenberg–Marquardt backpropagation method on this dataset. In the training process, the geometric parameters, wave vectors, and eige-order of the roots were used as the input information, and the eigenfrequencies were used as the target information in the first group of the dataset. Furthermore, the refractive index (n) of the main material was added to the second group of the dataset as additional information. In the second group of the dataset, the PCs made of glass with a refractive index of 1.5 were considered to compare with those made of silicon with a refractive index of 3.46. In the third group of the dataset, the honeycomb lattice PCs were considered with more variable geometric parameters for training.

The dataset used in the training process was obtained by the FEM and reconfigured to the form of the input matrix. We further calculated a BS of a PC that was not included in the training dataset to test the prediction ability of the trained ANN. The BSs calculated by the FEM and predicted by the ANN are compared.

2. Materials and Methods

A 2-D PC is formed by periodically arranging holes or pillars in the host material. With different arrangement methods, the PCs can be classified into several commonly used lattices, which include square lattices, triangular lattices, and honeycomb lattices. Figure 1a depicts the unit cell of a hole-type 2-D square lattice PC. The PC consists of air holes in a silicon host. The lattice constant and the radii of air holes are denoted by a and r, respectively. In practice, the structure can be realized by etching a silicon wafer with a thickness 10 times larger than the lattice constant. Figure 1b represents the reciprocal lattice of a 2-D square lattice. The first Brillouin zone and the reduced Brillouin zone are represented by the blue and pink areas in Figure 1b. The reduced Brillouin zone is obtained by reducing all of the symmetries in the first Brillouin zone in the point group of the lattice.

The BS was then solved within the reduced Brillouin zone to represent the dispersion in the whole crystal sufficiently.

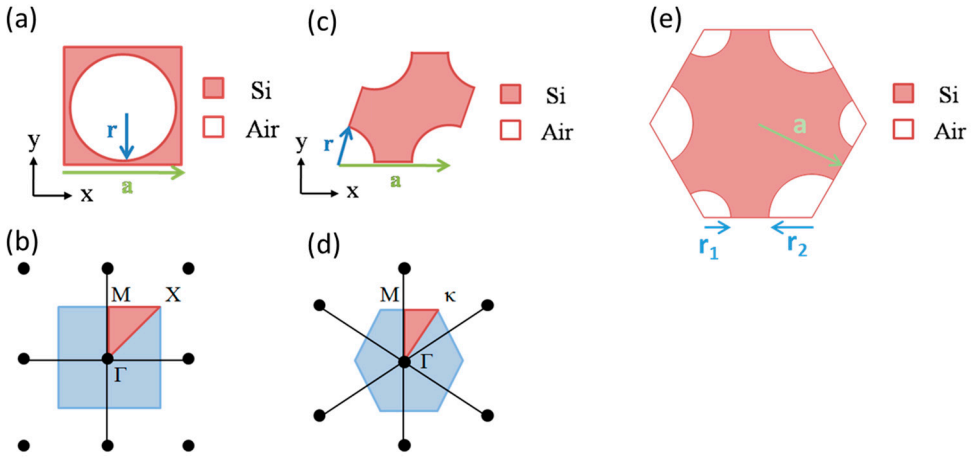

Figure 1. (**a**) Unit cell and (**b**) reciprocal lattice of 2-D square lattice photonic crystals. (**c**) Unit cell and (**d**) reciprocal lattice of 2-D triangular lattice photonic crystals. (**e**) Unit cell of 2-D honeycomb lattice photonic crystals.

On the other hand, the other commonly used arranging lattice type, the triangular lattice, is indicated in Figure 1c. The radii of the air holes and the lattice constant are denoted as r and a as well. Compared to the square lattice, a triangular lattice can generate a complete band gap more easily. However, the square lattice can provide a band gap for a certain polarization of light waves, while the triangular lattice may provide band gaps for both orthogonal polarizations [7]. In Figure 1d, the reciprocal lattice of the triangular lattice is shown by the black dots, and the first (blue) and reduced (pink) Brillouin zones are also shown in the sketch. With the same periodic lattice of the triangular lattice, the honeycomb-shaped lattice is formed by removing specific holes from the triangular lattice. Of the three of these commonly used lattices, the honeycomb lattice is known as the one that can produce a complete bandgap more easily than the others. Due to the special lattice configuration of the honeycomb lattice, its unit cell has two holes in the single unit cell rather than one that should be within the traditional unit cell.

In Figure 1e, the unit cell of the honeycomb lattice is depicted. The unit cell contains two holes in the single unit, meaning an additional radius can be manipulated. The lattice constant shown in Figure 1e is denoted by a as well, while the length is $\sqrt{3}$ times that of in the triangular lattice. The two sizes of the radii of the holes arranged at the endpoint of the hexagon are denoted by r_1 and r_2. Since the reciprocal lattice of the honeycomb lattice is similar to the triangular lattice but with different lengths of lattice constants, the calculation of the BSs is also very similar.

3. Results

3.1. Neural Networks for Band Structures of the Square Lattice and Triangular Lattice

The FEM-calculated BSs of the 2-D square lattice PC are shown in Figure 2a–d as blue circles. The r/a ratios of unit cells are shown at the top of each BS diagram. The horizontal axis of each BS represents the end point of the wave vectors, starting from the Γ point along the edge of the reduced Brillouin zone (red area) in Figure 1b to M, X, and back to the Γ point.

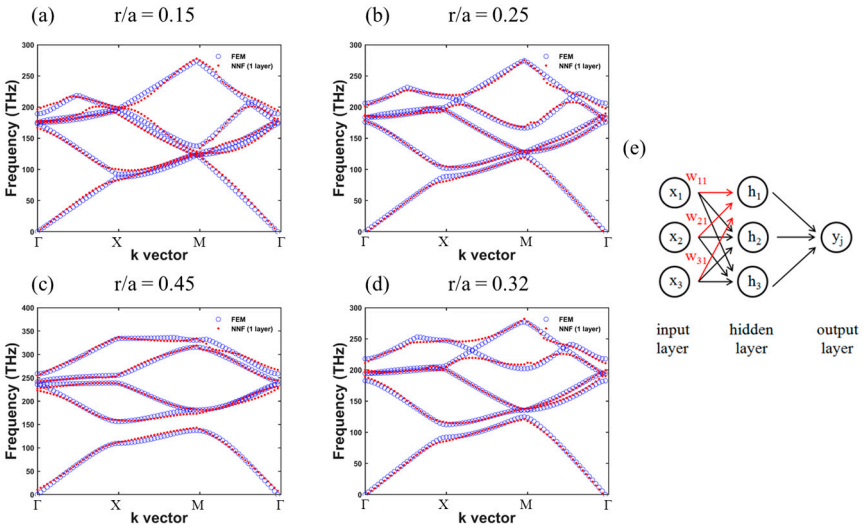

Figure 2. FEM-calculated (blue circles) and predicted (red dots) band structures of square lattice photonic crystals with r/a = (**a**) 0.15, (**b**) 0.25, (**c**) 0.45, and (**d**) 0.32. (**e**) Sketch of artificial neural network.

We only solved the lowest 5 eigenfrequencies in the BSs. In Figure 2a, r/a = 0.15, the band structure seems to only have four bands in the picture due to some eigenfrequencies calculated by the eigensolver being very close to each other in the higher frequency range. In fact, the mountain shape banding in the band with the highest frequency could be a cross-insertion of two bands going to the higher frequency range.

In order to train the ANN, we calculated all of the points in the BSs of the r/a ratio from 0.15 to 0.45, with an interval of 0.05. Based on the number of points in the BSs of different lattices, the total columns of data pairs listed in the datasets are $N_n \times N_{ra} \times N_{BS}$, where N_n is the number of refractive indices, N_{ra} is the number of the r/a ratio, and N_{BS} is the number of points in a single BS; for example, N_{BS} = 375 in the square lattice BSs. The details can be found in the supplemental data. The data of each point are collected and divided into two parts for training. One is the information of the wave vectors in the reduced Brillouin zone and the band numbers of each point in the BS, and the other part is the corresponding eigenfrequencies of each point.

Then, the eigenfrequencies are considered the target dataset of the ANN, and the rest of the data are considered the input dataset for training. The configuration of our ANN is sketched in Figure 2e. Five neurons represent the five rows of the dataset in the input layer, which are in the order of the length of the wave vector in the reduced Brillouin zone, the components of the wave vector in the Gamma-X and Gamma-M directions, the r/a ratio, and the band numbers. In the hidden layer, 10 neurons are set as the weights, and only 1 neuron is in the output layer. The data are separated into three groups randomly by the software, specifically the training set (70%), validation set (15%), and test set (15%). Between the full-connection neurons, backpropagation methods are used to train the weights within the hidden layer, and the performance of the ANN is evaluated by the mean square error.

The BS (red dots) predicted by the ANN are plotted with those calculated by the FEM. As can be seen in Figure 2a–c, the predicted eigenfrequencies agree well with those calculated results, and the correlation coefficient R = 0.99841. In Figure 2c, the BS also shows a complete band gap between the first and second bands. Due to the low-frequency location of the band gap, the bandgap information can be read in the predicted band structure as well as the FEM results. In Figure 2d, the BS of the PC with r/a =0.32 predicted by the ANN is depicted with those calculated by the FEM. From the BS of r/a = 0.32, we can find an opening gap between the first and second bands. Considering the complete band gap within the BS of r/a = 0.45, the gradually opened gap observed during the r/a varying process can be a hint of the existence of the band gap. Fortunately, this information can also be observed from the predicted results. It should be noted that this group of data

is not included in the training dataset. The predicted results then confirm the prediction performance of the ANN with just 10 neurons.

In Figure 3, the BSs of PCs arranged in a triangular lattice are depicted. The calculated eigenfrequencies of triangular lattice PCs were used as the training dataset as well, and the configuration of the ANN was kept the same as that for a square lattice. The training results are shown in Figure 3a–c. Based on the calculated points in blue circles, we can see that there are more mismatched points predicted by the ANN that appeared in the higher frequency range, and the correlation coefficient R decreased to 0.99529. This can be explained by the stronger frequency shift of the modes with higher frequency. The dramatic frequency shift in some bands at the Gamma point may increase the difficulty of the training process. Therefore, the mismatch is more serious in r/a = 0.45 than in the others. In Figure 3c, the triangular lattice PCs generate a complete band gap. Through the prediction results, the bandgap information can still be read in the predicted band structure, though the bandwidth is narrower than the true bandwidth.

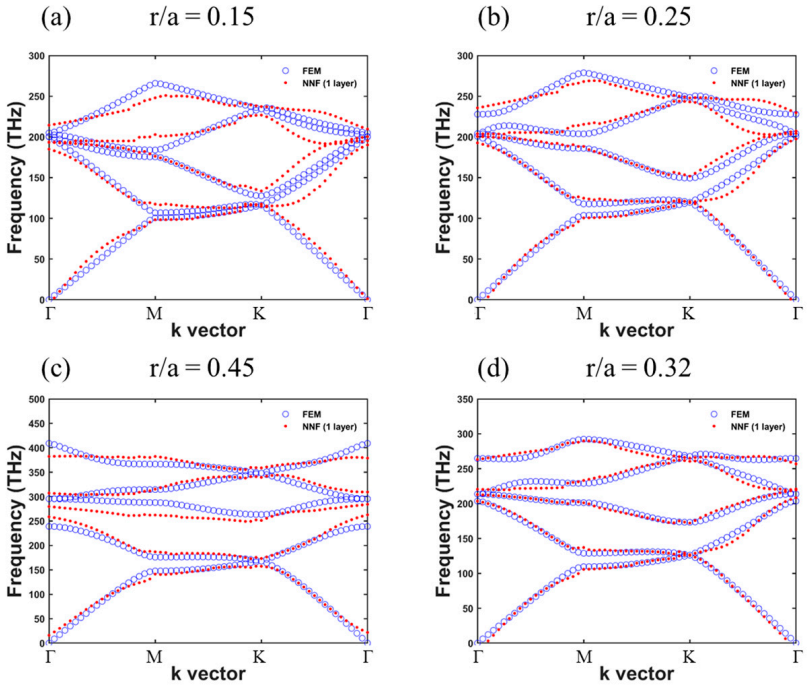

Figure 3. FEM-calculated (blue circles) and predicted (red dots) band structures of triangular lattice photonic crystals with r/a = (**a**) 0.15, (**b**) 0.25, (**c**) 0.45, and (**d**) 0.32.

Although the prediction results with higher frequencies show a few mismatches, the prediction result of r/a = 0.32 shown in Figure 3d, which is not included in the training dataset, still agrees well with the FEM-calculated results.

3.2. Refractive Index Discussion

The aforementioned PCs are set in the material silicon, which has a refractive index of 3.46. If the refractive index n is considered as input information, the neural network can further predict the BSs of PCs made of different materials. In order to further train the desired ANN, another group of BSs of PCs made of glass with the same r/a ratio as the silicon group was added to the dataset. The n information was added into the input matrix as the sixth neuron with a magnitude of 1.5 and 3.46, representing the refractive index of glass and silicon, respectively.

Figure 4 depicts the BSs of PCs made of silicon and glass in square lattices and triangular lattices with r/a = 0.45 in the four structures. The material that the PC is made of and the lattice arrangement are shown at the top of each BS diagram. The configuration of the ANN was set to be the same as the aforementioned one, and the input dataset and

target dataset were the only changed information. From the illustrations, we can find that 10 neurons in the ANN hidden layer are no longer enough to make predictions with this dataset with the refractive index information. The correlation coefficient of the net for square lattice decreased to 0.99286 and 0.99574 for triangular lattices. The band gap information in the predicted result also disappeared due to incorrect points.

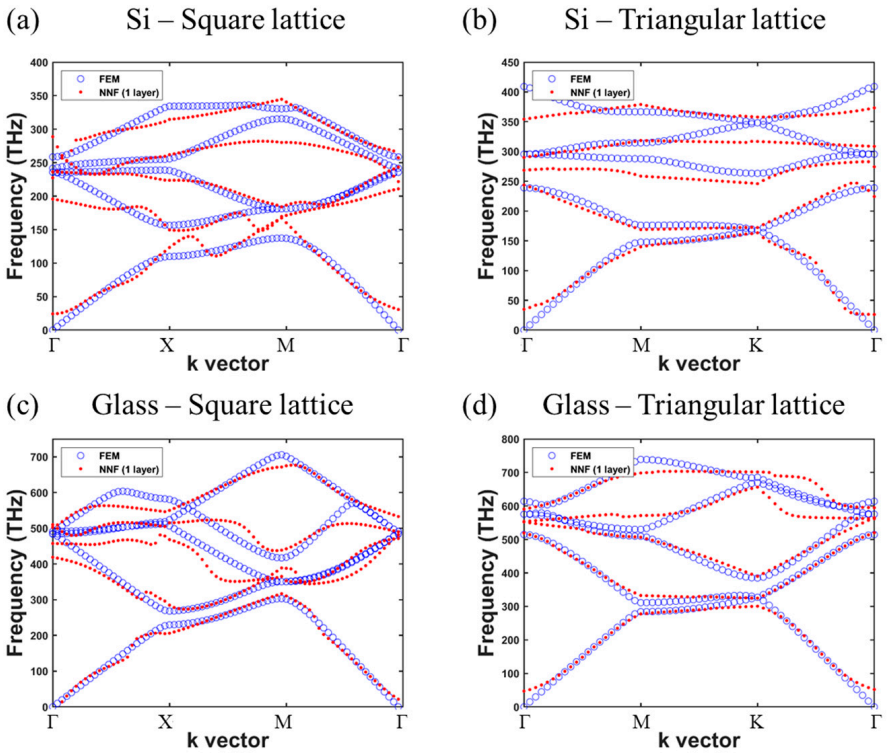

Figure 4. FEM-calculated (blue circles) and predicted (red dots) band structures of PCs made of Si in (**a**) square lattices and (**b**) triangular lattices and glass in (**c**) square lattices and (**d**) triangular lattices with r/a = 0.45 and 10 neurons in the hidden layer.

Comparing Figure 4a–d, the maximum eigenfrequency of the eigenmodes in the PC made of glass is almost double that made of silicon. The highest eigenfrequency of the fifth mode in Figure 4a,b is around 400 THz, while the highest eigenfrequency of the fifth mode in Figure 4c,d is around 750 THz. Under this huge data difference, the new dataset with double the number of data groups only acquires one additional piece of information containing only two values for the corresponding data, causing the prediction distortion in the original ANN configuration with a few neurons.

To resolve this issue, the number of neurons in the hidden layer was increased. The number of neurons can be chosen as a larger number, forming a further complex ANN. However, more neurons or even more hidden layers also cause more training time. Therefore, we set 25 neurons for appropriate predicted results and training time. The prediction results are shown in Figure 5. The same BSs with r/a = 0.45 were used to present the results. As can be seen in Figure 5, the accuracy in all four BSs in square lattices and triangular lattices was effectively optimized and even better than those prediction results formed by the original ANN. The correlation coefficient of the net for square lattices and triangular lattices increased to 0.99977 and 0.99979. In Figure 5b, the complete band gap information can be seen to be as clear as the FEM-calculated BS.

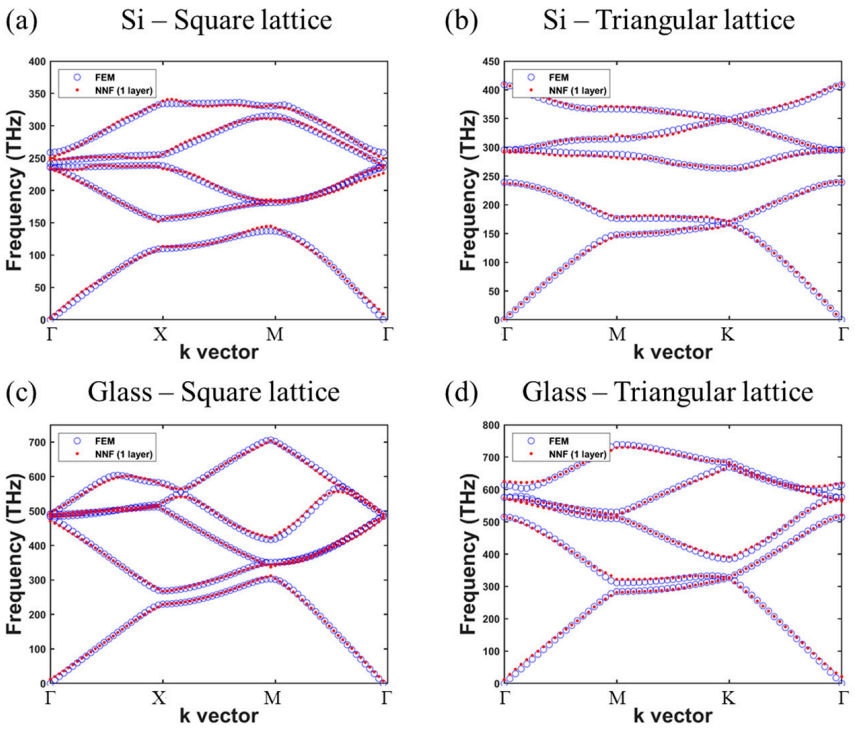

Figure 5. FEM-calculated (blue circles) and predicted (red dots) band structures of PCs made of Si in (**a**) square lattice and (**b**) triangular lattice and glass in (**c**) square lattice and (**d**) triangular lattice with r/a = 0.45 and 25 neurons in the hidden layer.

Using the optimized ANN, the BSs of the PC with r/a = 0.32 made of silicon and glass were set to confirm the accuracy. The refractive index, the length of the k vector, the components of the k vector in the Γ-X and Γ-M directions (Γ-M and Γ-K in the triangle lattice), the r/a ratio, and the band numbers were set as the input data matrix and fed to the trained ANN. In Figure 6, the band structures of the PC structures with r/a = 0.32 are depicted. Similar to the results in Figure 5, the predicted results plotted in red points fit well with the blue points calculated by the FEM.

Considering these data were not included in the training dataset, the results in Figure 6 prove the ability of the ANN in BS prediction not only for different geometric parameters in a specific PC but also for PCs made of different materials. It can be noted that the prediction results still have a few mismatching points appearing at the edge of the Brillouin zone, the bending curve, and the cross intersections.

A simple method to further optimize the prediction result is to increase the number of neurons in the hidden layers to be greater than the aforementioned ANN. However, the more complex the network configuration is, the more training time will be necessary as well. If the neurons in the hidden layer increase to 100 neurons, the correlation coefficient of the net for square lattice and triangular lattice both can be further increased to 0.99999, and the mismatching points will nearly disappear in this dataset but cost about 71 s. In contrast, training the final ANN with 25 neurons in a single hidden layer only costs about 12 s. Due to the small numbers of our datasets, the training time is very short. The huge training time difference between 100 neurons and 25 neurons shows that the configuration of the desired ANN can be wisely chosen to obtain enough accuracy with less training time.

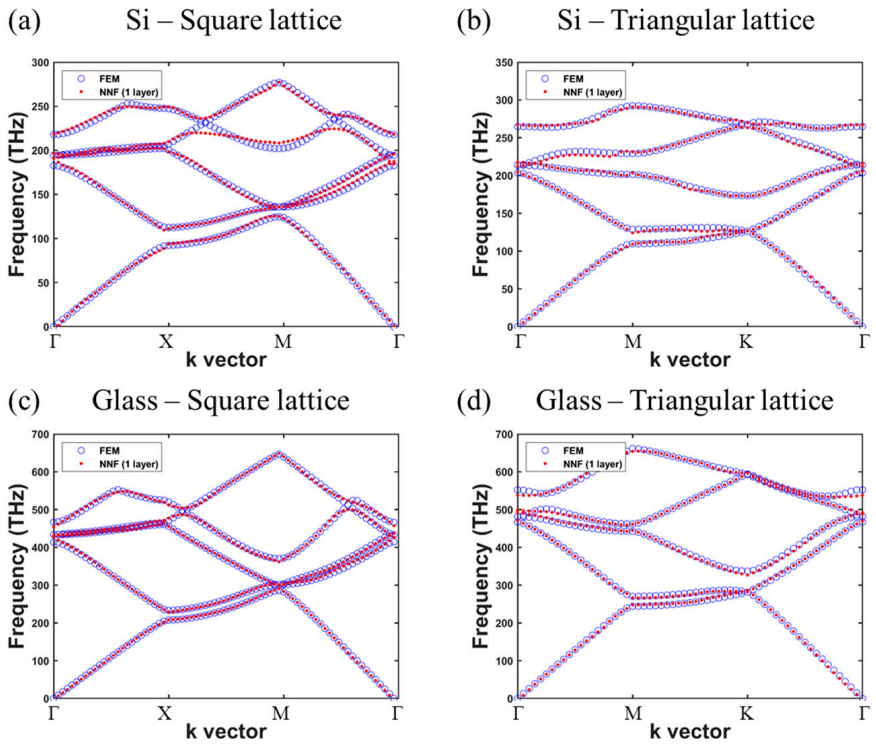

Figure 6. FEM-calculated (blue circles) and predicted (red dots) band structures of PCs made of Si in (**a**) square lattice and (**b**) triangular lattice and glass in (**c**) square lattice and (**d**) triangular lattice with r/a = 0.32 and 25 neurons in the hidden layer.

3.3. Honeycomb Lattice

After the discussion of the square lattice and triangular lattice, a different arrangement of PCs should be investigated, which is the honeycomb lattice. As mentioned in Section 2, the reciprocal lattice of the honeycomb lattice is similar to that of the triangular lattice. However, the radii of the two holes in the unit cell give an additional degree of freedom for bandgap manipulation. We calculated the BSs of both the r_1/a and r_2/a ratio from 0.15 to 0.45, with an interval of 0.05. A total of 49 groups of data were collected for training. The ANN with 25 neurons in a single hidden layer was used as the configuration for training.

In Figure 7, the band structures of the honeycomb lattice with different r_1/a and r_2/a pairs are depicted. In Figure 7a, both the r/a ratio of the holes are chosen to be 0.45 to present the training performance. As can be seen in the figure, the predicted results produced by the 25-neuron ANN fit well with those calculated by the FEM, shown in blue circles, and the correlation coefficient R = 0.99985. To confirm the prediction ability, the BSs are calculated by changing one or both the radii ratios of the holes to 0.32. In Figure 7b–d, the BSs of the honeycomb lattice PCs with r_1/a = 0.32 and r_2/a = 0.25, r_1/a = 0.4 and r_2/a = 0.32, and r_1/a = 0.32 and r_2/a = 0.32 are depicted, respectively. Through the figures, we can see the perfect prediction results in each pair of radii groups.

In Figure 7a–c, we can further find the band gaps that appear between the first and second bands and between the third and fourth bands. The band gap information can be read in the predicted band structure with almost the same bandwidth and center frequency as those calculated by the FEM. Although there are still a few mismatching points appearing at the bending point and a few frequency shifts in some of the points, the prediction results confirm the trained ANN has the power to handle the prediction of the BS.

It should be noticed that though the two PCs in Figure 7b,c have one of the radii within the range of r used for training, the data of all three groups of geometric pairs are not included in the training dataset. However, the difference between the PCs used in Figure 7b–d will occur in the inverse design process. Both well-predicted results with the dataset containing one unknown geometric parameter and two unknown parameters mean

that we can ask the ANN to design the PC devices with a certain geometric limitation or without the geometric limitation in the future.

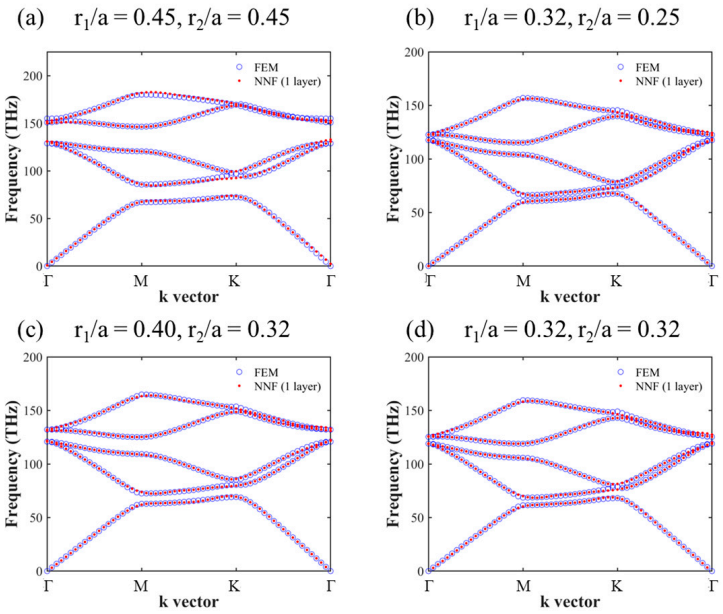

Figure 7. FEM-calculated (blue circles) and predicted (red dots) band structures of honeycomb lattice photonic crystals with (**a**) $r_1/a = 0.45$, $r_2/a = 0.45$, (**b**) $r_1/a = 0.32$, $r_2/a = 0.25$, (**c**) $r_1/a = 0.4$, $r_2/a = 0.32$, and (**d**) $r_1/a = 0.32$, $r_2/a = 0.32$.

4. Conclusions

We calculated the BSs of 2-D square lattice and triangular lattice PCs with different refractive indices. The information of the wave vectors, band numbers, and corresponding eigenfrequencies were used to train ANN for the square lattice PCs and the triangular lattice PCs. The prediction results show that the trained ANN with only 10 neurons can well predict the eigenfrequencies with an R over 0.99 according to the wave vectors in the reduced Brillouin zone, the r/a ratio, and the band numbers. However, when the refractive indices of the host material were added to the input dataset as additional information, the prediction quality decreased due to the huge differences between the data of these different refractive indices. After increasing the number of neurons in the ANN to 25, the accuracy obviously increased, and the correlation coefficient effectively increased to over 0.999. However, it should be noticed that the more complex the configuration of the ANN is, the greater the training time will be. Wisely choosing the appropriate neurons in the hidden layer to obtain acceptable results will effectively save training time.

Using the optimized ANN, the BSs of 2-D honeycomb lattice PCs were considered the input dataset. The special spatial configuration of the unit cell gives an additional degree of freedom for geometric manipulation. The prediction results in those with one unknown geometric parameter and two unknown parameters fit well with the FEM. The results present more possibilities to design PC devices by a trained ANN inversely with a specific geometric limitation or without a geometric limitation in the future.

Supplementary Materials: The following supporting information can be downloaded at: https://www.mdpi.com/article/10.3390/electronics12081777/s1.

Author Contributions: Conceptualization, F.-L.H.; methodology, F.-L.H., H.-F.L. and Y.-P.T.; software, F.-L.H., H.-F.L.; validation, F.-L.H., H.-F.L. and Y.-P.T.; formal analysis, F.-L.H., H.-F.L. and S.-C.W.; investigation, F.-L.H., H.-F.L. and Y.-M.W.; resources, F.-L.H.; data curation, H.-F.L. and Y.-P.T.; writing—original draft preparation, F.-L.H., H.-F.L. and S.-C.W.; writing—review and editing, F.-L.H. and Y.-P.T.; visualization, H.-F.L. and S.-C.W.; supervision, F.-L.H. and Y.-P.T.; project administration, F.-L.H. and Y.-P.T. All authors have read and agreed to the published version of the manuscript.

Funding: This research received no external funding.

Data Availability Statement: Not applicable.

Conflicts of Interest: The authors declare no conflict of interest.

References

1. Yablonovitch, E. Photonic Crystals. *J. Mod. Opt.* **1993**, *41*, 173–194. [CrossRef]
2. John, S. Strong localization of photons in certain disordered dielectric superlattices. *Phys. Rev. Lett.* **1987**, *58*, 2486. [CrossRef] [PubMed]
3. Wu, L.; He, S.; Shen, L. Band structure for a one-dimensional photonic crystal containing left-handed materials. *Phys. Rev. B* **2003**, *67*, 235103. [CrossRef]
4. Yang, G.; Yu, S.; Dong, H.; Slabaugh, G.; Dragotti, P.L.; Ye, X.; Liu, F.; Arridge, S.; Keegan, J.; Guo, Y.; et al. DAGAN: Deep De-Aliasing Generative Adversarial Networks for Fast Compressed Sensing MRI Reconstruction. *IEEE Trans. Med. Imaging* **2018**, *37*, 1310–1321. [CrossRef] [PubMed]
5. Jin, K.H.; McCann, M.T.; Froustey, E.; Unser, M. Deep Convolutional Neural Network for Inverse Problems in Imaging. *IEEE Trans. Image. Process.* **2017**, *26*, 4509–4522. [CrossRef]
6. Yoo, J.; Sabir, S.; Heo, D.; Kim, K.H.; Wahab, A.; Choi, Y.; Lee, S.-I.; Chae, E.Y.; Kim, H.H.; Bae, Y.M.; et al. Deep Learning Diffuse Optical Tomography. *IEEE Trans. Med. Imaging* **2019**, *39*, 877–887. [CrossRef]
7. Joannopoulos, J.D.; Johnson, S.G.; Winn, J.N.; Meade, R.D. *Photonic Crystals–Molding the Flow og Light*, 2nd ed.; Princeton University Press: Princeton, NJ, USA, 2008; pp. 66–93.